J Comput Aided Mol Des (2013) 27:975–987
DOI 10.1007/s10822-013-9694-y

Investigating the hydrogen-bond acceptor site of the nicotinic pharmacophore model: a computational and experimental study using epibatidine-related molecular probes

Clelia Dallanoce · Giovanni Grazioso · Diego Yuri Pomè · Miriam Sciaccaluga · Carlo Matera · Cecilia Gotti · Sergio Fucile · Marco De Amici

Received: 14 August 2013 / Accepted: 19 November 2013 / Published online: 26 November 2013

Abstract The binding mode of nicotinic agonists has been thoroughly investigated in the last decades. It is now accepted that the charged amino group is bound by a cation-π interaction to a conserved tryptophan residue, and that the aromatic moiety is projected into a hydrophobic pocket deeply located inside the binding cleft. A hydrogen bond donor/acceptor, maybe a water molecule solvating this receptor subsite, contributes to further stabilize the nicotinic ligands. The position of this water molecule has been established by several X-ray structures of the acetylcholine-binding protein. In this study, we computationally analyzed the role of this water molecule as a putative hydrogen bond donor/acceptor moiety in the agonist binding site of the three most relevant heteromeric (α4β2, α3β4) and homomeric (α7) neuronal nicotinic acetylcholine receptor (nAChR) subtypes. Our theoretical investigation made use of epibatidine **1** and deschloroepibatidine **2** as molecular probes, and was then extended to their analogues **3** and **4**, which were subsequently synthesized and tested at the three target receptor subtypes. Although the pharmacological data for the new ligands **3** and **4** indicated a reduction of the affinity at the studied nAChRs with respect to reference agonists, a variation of the selectivity profile was clearly evidenced.

Keywords Neuronal nicotinic acetylcholine receptors · Epibatidine and analogues · Docking · Molecular dynamics · Target-based drug design · Binding affinity · Functional potency and selectivity

Introduction

Neuronal nicotinic acetylcholine receptors (nAChRs), which belong to the superfamily of ligand-gated ion channels with a pentameric structural architecture, are widely distributed in the human central nervous system (CNS), where they modulate the release of almost all the neurotransmitters and mediate the synaptic transmission in a few selected areas [1]. The differential assembly of homologous, genetically distinct α and β subunits (α2–α10 and β2–β4) dictates the functional properties of individual channels, including cation permeability, activation and desensitization kinetics as well as ligand pharmacology [2–5]. Neuronal nAChRs, which are selectively activated by the alkaloid (*S*)-(−)-nicotine, are critically involved in processes such as cognition, learning and memory, cerebral blood flow and metabolism. At present, they are under consideration for therapeutic intervention in an array of

Electronic supplementary material The online version of this article (doi:10.1007/s10822-013-9694-y) contains supplementary material, which is available to authorized users.

C. Dallanoce · G. Grazioso (✉) · D. Y. Pomè · C. Matera · M. De Amici
Sezione di Chimica Farmaceutica "Pietro Pratesi", Dipartimento di Scienze Farmaceutiche, Università degli Studi di Milano, Via L. Mangiagalli 25, 20133 Milan, Italy
e-mail: giovanni.grazioso@unimi.it

M. Sciaccaluga · S. Fucile
Istituto Neurologico Mediterraneo I.R.C.C.S. Neuromed, Via Atinese 18, 86077 Pozzilli, Isernia, Italy

C. Gotti
Dipartimento di Biotecnologie Mediche e Medicina Traslazionale, CNR, Istituto di Neuroscienze, Università degli Studi di Milano, Via Vanvitelli 32, 20129 Milan, Italy

S. Fucile
Dipartimento di Fisiologia e Farmacologia, Università di Roma La Sapienza, Piazzale A. Moro 5, 00185 Rome, Italy

pathological conditions such as Alzheimer's and Parkinson's diseases, schizophrenia, epilepsy, Tourette's syndrome, anxiety, depression, pain and nicotine addiction [6–8].

In the last decade, the rational design of ligands for a selected nAChR subtypes took advantage of the identification of structural analogies and differences among receptor/ligand complexes as well as the application of computational approaches enabling an accurate quantitative estimation of pivotal ligand-receptor interactions. The availability of crystal structures of invertebrate acetylcholine-binding proteins (AChBPs), such as those derived from *Aplysia californica* (*A*-AChBP) [9], *Lymnaea stagnalis* (*L*-AChBP) [10] and, more recently, *Capitella teleta* (*Ct*-AChBP) [11], has provided valuable models to investigate the structural determinants for the molecular recognition of ligands by nAChRs. The 3D arrangements of various full agonists, partial agonists and antagonists, mainly co-crystallized with the above cited AChBPs, which are soluble pentameric analogous of the *N*-terminal extracellular ligand-binding domain of the Cys-loop family of receptors, have been exploited as templates for the elaboration of homology models of homopentameric and heteropentameric nAChR subtypes, thus substantially improving the target-based design of subtype-selective nicotinic ligands [12–15].

Agonists sharing the same structural motif of (*S*)-(−)-nicotine, i.e., a positive charged head connected to an aryl moiety, bind at subunit interfaces, adopting similar binding modes in the nAChR recognition crevice [10] For heteromeric nAChRs, a major contribution of the binding interaction involves the charged nitrogen atom with an "aromatic box" belonging to an α subunit, surrounded by the side chains of several conserved residues. Here, the carbonyl oxygen atom of a conserved Trp residue produces a hydrogen bond with the same charged cationic head. In addition, a complementary agonist-binding site exploits a hydrogen bonding interaction with the secondary hydrogen bond acceptor site of agonists (e.g., the pyridine nitrogen of nicotine or the carbonyl group of ACh) [10]. The structure-affinity relationships of numerous nicotinic agonists allow to conclude that a hydrogen bond acceptor moiety on the aromatic ring of the ligand is required for an accessorial, productive interaction with the complementary receptor protein, and this contact could be mediated by a water molecule. Computational and experimental investigations performed by Amiri et al. [16] and, recently, by Blum et al. [17, 18] indicated the presence and clarified the role of several water molecules in the nAChR binding cleft, suggesting that some of them could be replaced by an equivalent moiety belonging to the ligand molecular skeleton.

In this study, at first we evaluated by molecular modeling investigations the putative role of a water molecule in affecting the binding mode of epibatidine, a reference nAChR agonist endowed with very high affinity and agonist potency but lacking subtype selectivity [19]. Initially, we inserted epibatidine **1** and its analogue deschloroepibatidine **2** (Fig. 1) within the models of the active site of the α4β2, α7 and α3β4 nicotinic channels, i.e. the most relevant neuronal nAChR subtypes expressed in the human CNS [19, 20]. The two reference compounds were analyzed by docking experiments and molecular dynamics (MD) simulations. Then, we extended our theoretical investigation to derivatives **3** and **4** (Fig. 1), designed as close analogues of **2**, whose 3′-hydroxyl and 3′-hydroxymethyl moieties are theoretically capable of mimicking a water molecule in mediating the ligand-receptor recognition process in the auxiliary subsite of the nicotinic pharmacophore. As a reference structure, we have also inserted in Fig. 1 the active enantiomer of *N*-methyl-2-phenylpyrrolidine [(*S*)-MPP, **5**] [17], the analogue of nicotine in which benzene replaced the pyridine ring. The two novel nicotinic ligands **3** and **4** were then synthesized and tested at the three target nAChRs, thus disclosing a propensity for a preferential interaction with the α3β4 receptor subtype.

Results

Molecular modeling

Investigation of the role of water molecules on the binding of known agonists

The X-ray crystal structure of epibatidine (1*R*,2*R*,4*S*)-**1** within the *A*-AChBP (PDB accession code 2BYQ), reported by Hansen et al. [9], exemplifies the molecular interactions involving nicotinic agonists in the binding cleft. Worth noting, the charged amino group of **1** is accepted by an "aromatic box" surrounded by the side chains of Trp147 and four Tyr residues (55, 93, 188 and 195), whereas a hydrogen bond between the carbonyl oxygen of Trp147 and the same charged head directs the pyridine ring in a hydrophobic pocket shaped by Ala107, Val108, Ile118 and Val148. Although this crystal structure doesn't include any water molecules, probably due to their lack of order in the binding cleft, the authors hypothesized that the pyridine nitrogen should bind to the backbone of Ile118 by a putative water molecule [9]. The presence of water molecules is a matter of debate because computational studies making use of docking calculations should take into account also such a hydrogen bond donor/acceptor site [21].

To investigate the presence and the role of water in the binding of **1** and of structurally related compounds, we performed computational studies using our molecular models of the α4β2 [22] and α7 [23] nAChR subtypes, and the recently elaborated α3β4 variant [14]. Initially, we placed **1**, which is a high-affinity agonist for the three investigated subtypes, at the orthosteric interfaces with a

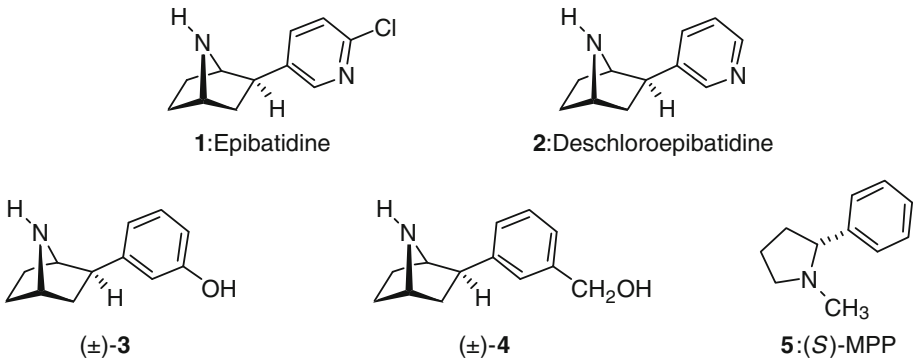

Fig. 1 Molecular structures of reference and novel ligands in this study

binding pose matching that observed in the crystal structure of the *A*-AChBP/**1** [9] complex. A water molecule linking the backbone of the residues corresponding to Leu102 and Met114 of *L*-AChBP/nicotine (PDB accession code 1UW6) [10] was then inserted in a homologue position of the three nAChR models. The quality of the complexes built with **1** and the water molecule within the nAChR models was improved by means of energy minimization, equilibration and MD simulations, which allowed the systems to attain the geometrical stability (see "Experimental section"). In the three **1**/nAChR complexes, at the end of MD simulations (more than 10 ns) the water molecule and the nicotinic agonist **1** were found to be located in different mutual positions, if the acquired geometries were compared with the starting ones. As far as the α4β2 complex is taken into account, the mobility of the solvent molecule allowed the setting up of a hydrogen bond network mainly involving the backbone oxygen atom of β2-Leu119, the carbonyl group of β2-Asn107, occasionally the amino group of β2-Leu119, and the pyridine nitrogen atom of **1** (Fig. 2). This simulation indicated that the water molecule is not firmly bound to the nitrogen atom of β2-Leu119 but its interaction with the oxygen atoms of the same residue is better stabilized. This evidence is in line with the results of Blum et al. [17] who ascertained that removal of the NH group of β2-Leu119, following the β2-Leu119Lah (Lah being α-hydroxyleucine) mutation, caused less than three-fold reduction of the EC_{50} value measured for **1**, at variance with those of other studied nicotinic agonists, which were more significantly affected. Moreover, (*S*)-MPP (**5**, Fig. 1) showed higher efficacy in the presence of the *Lah* mutation, highlighting that a perturbation of the water molecule hydrogen bond network compromises the hydrophilic environment hosting the pyridine ring lone pair [17]. In this respect, (*S*)-MPP was used as a probe to evaluate the binding mode of a group of nicotinic agonists containing a hydrogen bond acceptor site. The authors didn't unequivocally establish that a water molecule is located in the binding site, however its presence was found to be compatible with the reported experimental data [17].

If the parallel computational results on the α3β4/**1** complex are considered, the hydrogen bond created by the water molecule has a similar pattern compared to that observed in the α4β2 model. However, a difference exists in the protein backbone atoms involved in the interaction of the water molecule. In fact, we found that the β2-Thr106 replaced the β2-Asn107 in the coordination of the water molecule. Moreover, the pyridine nitrogen of **1** (NPyr) was now the preferred hydrogen bond acceptor site since, as shown in Fig. 2, the distance between NPyr and the water oxygen in the α3β4 model is stabilized around optimal values of 3 Å throughout the simulation time. Conversely, in the α4β2/**1** complex the ligand NPyr flips around four different hydrogen bond donor/acceptor sites during the molecular dynamics simulations.

On the other hand, in the α7/**1** complex, the water molecule, adopting the initial binding mode, was found to be tightly bound to the pyridine nitrogen of **1** as well as the backbone atoms of Leu and Asn residues.

By careful evaluation of the MD simulation trajectories, we concluded that the water molecule plays a significant role in the process of molecular recognition of **1**, owing to its stability in the binding sites of the studied nAChR stoichiometries. However, further investigations should be carried out to account for the binding mode of other nicotinic agonists when solvent molecules are present within the binding cleft. Thus, we further considered deschloroepibatidine (1*R*,2*R*,4*S*)-**2** (Fig. 1), a close analogue of epibatidine whose affinity (K_i = 8.5 pM) is even higher than that reported for **1** (K_d = 30 pM) at α4β2 nAChRs but not at the α3β4 subtype (K_i = 11,000 pM vs. K_d = 300 pM for **2** and **1**, respectively) [24]. As for nicotine, **2** contains a pyridine ring, which has a pK_a value five orders of magnitude higher than the 2-chloropyridine moiety belonging to **1** [25]; therefore **2** is expected to behave as a better hydrogen bond acceptor than **1**. Accordingly, the computational approach previously carried out on **1** was extended to **2**, and the MD simulation profiles of the three nAChR/**2** models showed that, for the α4β2 and α7 subtypes, the water molecule was strongly associated to the pyridine nitrogen of **2** and to the amide and carbonyl groups of Leu and Asn residues, respectively. As expected, the absence of the

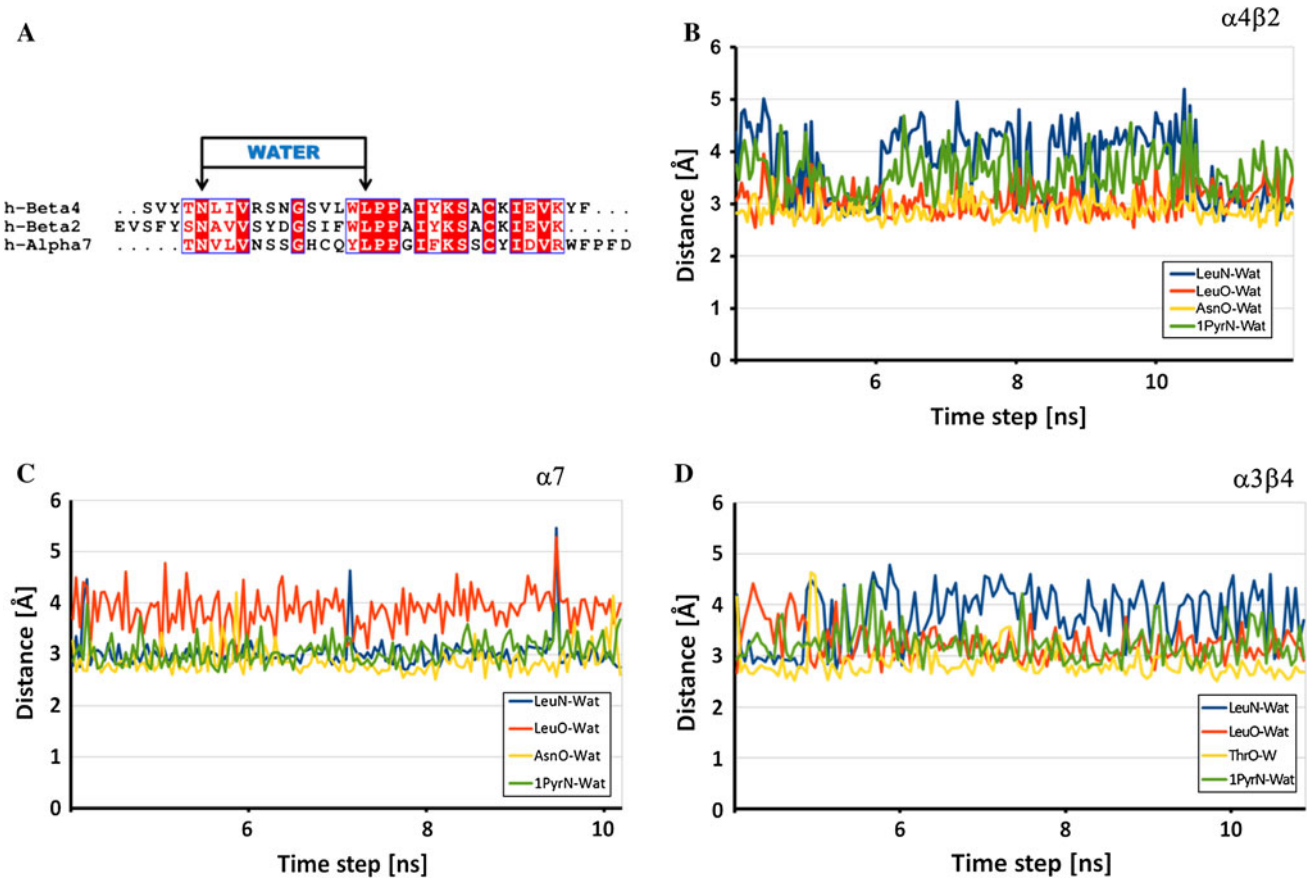

Fig. 2 **a** Alignment of the human β4, β2 and α7 sequences. The *arrows* highlight the residues involved in the stabilization of the water molecule. **b**, **c**, **d** Fluctuation of the hydrogen bond distances created by the water molecule in the binding site of α4β2, α7 and α3β4 models in complex with **1**

halogen atom in the molecular structure of **2** enhanced the interaction of the ligand with the solvated receptor binding site, the pyridine ring being a stronger hydrogen bond acceptor than the 2-chloropyridine counterpart of **1**.

In analogy to what observed for the α3β4/**1** complex, in the α3β4/**2** complex a new hydrogen bond linkage was evidenced, which involves the water molecule and a subsite sized by the side chain of α3-Trp149 and the carbonyl oxygen atoms of β4-Leu119 and β4-Thr106, the latter replacing the β4-Asn107 interaction. Moreover, at the end of simulations, the pyridine ring of **2** lost the initial interaction with the water molecule (Fig. 3a), being flipped by 180° with respect to the starting binding mode. As a consequence, in the α3β4 subtype, the water molecule and **2** are stabilized in a distinct site and adopt a different binding mode (Fig. 3b) than those assumed by the other simulated nAChR/**2** complexes.

Designing analogues of epibatidine

Based on the above discussed computational results, we designed new ligands putatively able to perturb the water-mediated network of hydrogen bonding. Due to the different location of the water molecule in the α4β2 and α3β4 binding sites of complexes with **1** and **2**, suitably designed analogues able to affect the solvent interactions within the binding pocket could be endowed with novel affinity, selectivity and functional profiles. A strategy to influence the water location is to anchor moieties mimicking the water structure to the skeleton of ligand molecules. This approach has been successfully adopted to increase the binding affinity of a group of HIV-1 protease inhibitors [26].

As it has been already shown in Fig. 1, we designed the two derivatives **3** and **4**, in which the 3′-pyridinyl ring of **2** has been substituted by the 3′-hydroxybenzene or 3′-hydroxymethylbenzene moieties. In the new ligands, the distance between the aromatic carbon atom, replacing the pyridine nitrogen, and the oxygen atom, simulating the water molecule, is 1.4 Å (**C–OH** for **3**) and 2.4 Å (**C–CH_2OH** for **4**), respectively. As a result, the –OH and the –CH_2OH groups of the new ligands are not capable to replace the water molecule in the orthosteric site because the optimal distance should be close to 2.8 Å. In fact, this distance, measured in each of the twenty binding sites of the X-ray structure of nicotine within *L*-AChBP, spanned the range 2.6–3.0 Å [10].

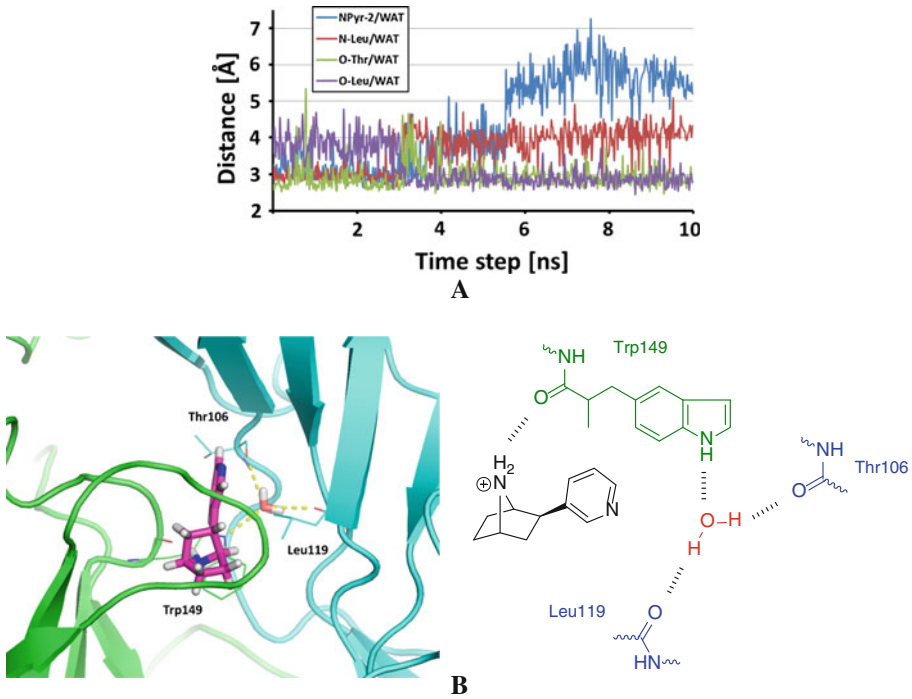

Fig. 3 **a** MD simulations on the **2**/α3β4 complex: distance fluctuation between the water oxygen atom and the backbone of β4-Leu119, β4-Thr106, α3-Trp149 and the pyridine nitrogen of **2**. **b** Hypothetical binding mode of **2** within the α3β4 binding site

To preliminarily verify these hypotheses, docking analyses and MD simulations were performed on the new ligands **3** and **4** within the α3β4 and α4β2 nAChR molecular models, i.e. the subtypes at which the model agonists **1** and **2** bind with the highest affinity.

Docking and MD simulations of designed compounds

As reported above, preliminary docking and MD simulations were accomplished on the α3β4 and α4β2 nAChR models for (1*R*,2*R*,4*S*)-**3** and (1*R*,2*R*,4*S*)-**4**, which match the stereochemistry of the active isomer of **2** [20]. We omitted the parallel study on the α7 model, due to the unavailability of experimental affinity data of **2** on this receptor subtype. Within the α3β4 nAChR model, ligand **3** adopted a binding mode involving: (1) a cation-π interaction between the charged amino group and the aromatic residue surrounding the α3-Trp149, (2) a hydrogen bond connecting the same charged head and the side chains of α4-Tyr93, and (3) a hydrogen bond between the ligand OH group and a water molecule firmly bound to the backbone of β4-Asn107 (Fig. 4a), close to the side chain of the α3-Ser150, a residue corresponding to Thr148 in the α4 primary structure. Therefore, although the OH moiety of **3** was unable to mimic the water molecule, the ligand apparently prevented the hydrogen bonding network involving water and the backbone of β2-Leu119.

Conversely, in the α3β4/**4** complex a water molecule mediated the interaction between the NH group of β4-Leu119 and the CO group of β4-Thr106, while the CH_2OH moiety was placed close to the side chain of the latter residues (Fig. 4b). Moreover, the presence of the ligand CH_2OH group suppressed the water molecule interaction with the side chain of α3-Trp149, whereas the charged amino group was typically connected to the side chains of α3-Tyr93 and the carbonyl group of α3-Trp149. Thus, our virtual analysis on the two novel nicotinic ligands **3** and **4** evidenced a different interaction with the water molecule located in the α3β4 binding site and, at the end of MD simulations, the two derivatives adopted distinct binding modes, each deviating from the binding mode predicted for **2**.

Different results were obtained when the model of the α4β2 subtype was investigated. In fact, in the theoretical binding mode of **3**, the aryl moiety was rotated by 180° with respect to the conformation of the pyridine ring observed in our simulations for **2**, or that established by X-ray analysis for **1**. Moreover, the same ligand was unable to displace the putative water molecule present in the α4β2 binding site due to hydrogen bonds alternatively generated by **3** with the side chains of α4-Tyr197 and β2-Arg81 (not shown), as deduced by considering the MD simulation trajectories.

On the other hand, in the binding mode acquired by **4** (Fig. 5), the hydroxymethyl group was oriented toward the side chain of α4-Glu195, i.e. opposite to the putative water binding site, while the charged amino group preserved the classical motif of interactions typical of reference ligands **1** and **2**.

On the whole, the above discussed computational investigations suggest that both **3** and **4** are able to perturb

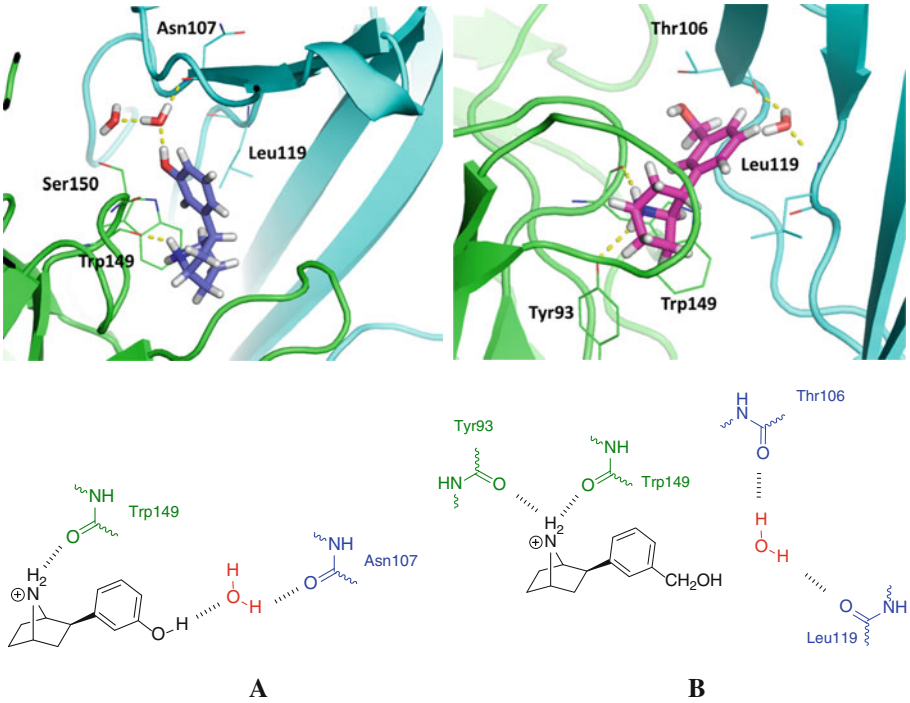

Fig. 4 Binding modes of compounds **3** (*blue*, **a**) and **4** (*magenta*, **b**) into the α3β4 nAChR homology model at the end of MD simulations. The residues involved in the ligand binding are represented as *thin sticks*, and are *colored* in *green* (α3 chain) and cyan (β4 chain)

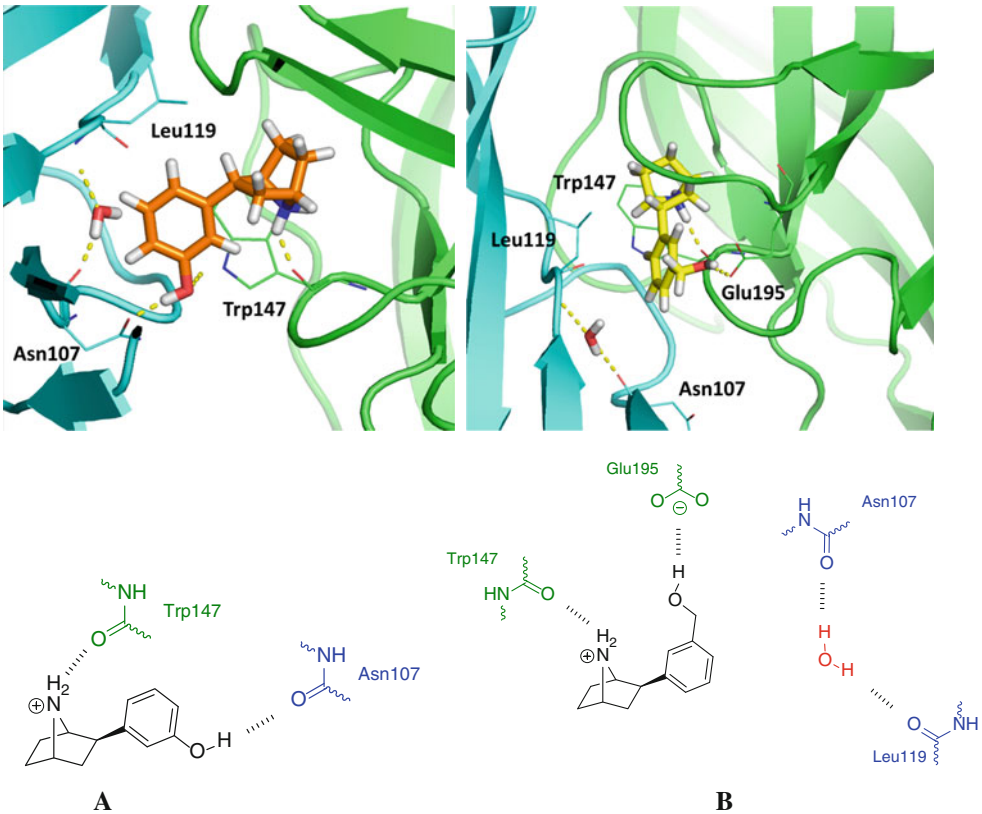

Fig. 5 Compounds **3** (*orange*, **a**) and **4** (*yellow*, **b**) binding to the α4β2 nAChR. The β2 and α4 chains are *colored cyan* and *green*, respectively. The residues involved in the ligand binding are represented as *thin sticks*

the receptor subsite of the α3β4 subtype in which the putative water molecule was initially bound, causing a different pose of the two ligands compared to the binding mode of their analogues **1** and **2**. Conversely, the same study performed on the α4β2 receptor model highlighted a more drastic modification of the mutual ligand-receptor interactions, since the binding mode of **3** and **4** was substantially different with respect to that adopted by the

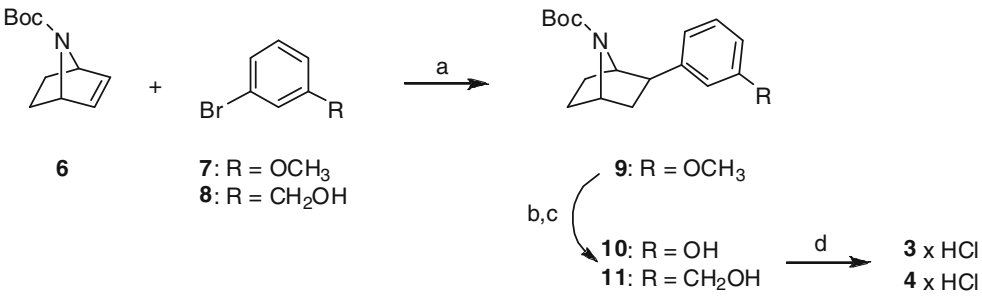

Scheme 1 Reagents and conditions: (*a*) $Pd(OAc)_2$, $(C_4H_9)_4N^+Cl^-$, HCOOK, DMF, 80 °C, 7 h; (*b*) 1 M BBr_3/hexane (2.2 equiv), CH_2Cl_2, −78 °C, 1 h, then 0 °C, 2 h; (*c*) $(Boc)_2O$ (2 equiv), Et_3N (pH 9), CH_2Cl_2, rt, 2 h; (*d*) 4 N HCl/dioxane (10 equiv), Et_2O, rt, 4 h

model nicotinic agonist **2**. In the light of these results, we decided to synthesize derivatives **3** and **4** and evaluate their pharmacological profile at the three nAChR subtypes explored in the theoretical investigation.

Chemistry

The racemates of 3′-hydroxybenzene and the 3′-hydroxymethylbenzene deschloroepibatidine analogues **3** and **4** were prepared as shown in Scheme 1. Reductive palladium acetate-catalyzed addition of 1-bromo-3-methoxybenzene **7** to 7-*tert*-butoxycarbonyl-7-azabicyclo[2.2.1]hept-2-ene **6** [27] in DMF containing tetrabutylammonium chloride and potassium formate at 80 °C [28] provided the intermediate 7-*tert*-butoxycarbonyl-2-*exo*-(3′-methoxyphenyl)-7-azabicyclo[2.2.1]heptane **9**. We assigned the *exo* configuration to the adduct **9** by considering the outcome of reductive Heck coupling reactions on bicyclic olefins structurally related to **6** [29]. According to the above described procedure, the palladium acetate-catalyzed reaction of 3-bromobenzyl alcohol **8** with **6** produced 7-*tert*-butoxycarbonyl-2-*exo*-(3′-hydroxymethylphenyl)-7-azabicyclo[2.2.1]heptane **11**. Treatment of **9** with a 1.0 M solution of boron tribromide/hexane in dichloromethane caused the *N*-Boc cleavage in addition to the desired *O*-demethylation, giving rise to a water soluble amino alcohol, which we were unable to purify. Hence, the same protective group was promptly reinserted to afford the *tert*-butoxycarbonyl-protected 3′-hydroxyphenyl intermediate **10**. Finally, conversion of the *N*-Boc intermediates **10** and **11** into the corresponding hydrochlorides of secondary amines **3** and **4** was achieved by treatment with a 4 N solution of HCl in dioxane (Scheme 1).

Pharmacology

The target compounds **3** and **4** were tested for their binding affinity at rat α7 and α4β2 nAChRs using [^{125}I]-α-bungarotoxin and [^{3}H]-epibatidine as radioligands, respectively. [^{3}H]-epibatidine was also the chosen radioligand to evaluate the binding affinity of **3** and **4** at heterologously expressed α3β4 nAChRs (Table 1). The K_i values, calculated from the competition curves of three separate experiments by means of the LIGAND program [30], are gathered in Table S2 (see Supplementary Material) and compared with those of reference analogues epibatidine **1**, deschloroepibatidine **2**.

Table 1 Radioligand binding data for reference and target compounds

Compounds	α4β2 K_i (nM) (% CV)	α7 K_i (nM) (% CV)	α3β4 K_i (nM) (% CV)	α4β2 versus α3β4 selectivity
1	0.030[a]	16/22[b]	0.3[a]	10
2	0.0085[a]	NA[c]	11[a]	1,290
3	127 (11)	609 (36)	80 (26)	0.63
4	429 (14)	1,800 (35)	92 (24)	0.21

The K_i values of **3** and **4** were derived from three competition binding experiments. The numbers in brackets refer to the % coefficient of variation. Literature data available for the racemic mixture of **1** and **2** have been also included

[a] K_d value taken from Refs. [19, 41]

[b] Binding affinity data of (−) and (+) isomers of epibatidine **1**, Ref. [42]

[c] *NA* not available

As previously mentioned, epibatidine **1** displays an exceptionally high affinity at the nAChRs under study, notably at the α4β2 subtype ($K_d = 0.030$ nM). The chlorine atom on the pyridine ring is not crucial to the affinity of **1** at the same nicotinic channel, since the affinity value of deschloroepibatidine **2** ($K_i = 0.0085$ nM) is quite similar to that measured for the parent, natural ligand. As reported in Table S2, the novel epibatidine-related hydroxyl-containing derivatives **3** and **4** are characterized by a substantial loss of affinity as compared with the two reference agonist ligands **1** and **2**. As a matter of fact, compounds **3** and **4** show affinities in the low micromolar range ($K_i = 127$ and 429 nM, respectively) at the α4β2 receptor, and, to a lesser extent, lose affinity even at the homomeric α7 and heteromeric α3β4 subtypes. However, the molecular recognition of **3** and **4** by the α3β4 receptor ($K_i = 80$ and 92 nM, respectively) is still remarkable and a preference for this channel has been gained, although with a poor subtype selectivity.

We further characterized the 3′-hydroxybenzene derivative **3** in electrophysiological experiments to assess its

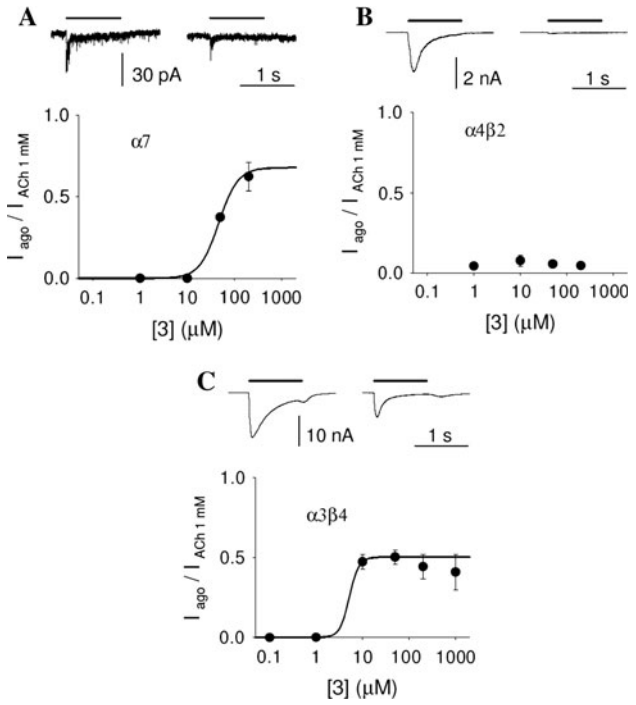

Fig. 6 Compound **3** elicits inward currents in GH4C1 cells transfected with human α7, α4β2 and α3β4 nAChRs. **a** *Top*, typical whole-cell currents elicited by ACh 1 mM and compound **3** 200 μM (*left* and *right*, respectively; *horizontal bars* represent agonist applications; holding potential, −70 mV) on GH4C1 cells expressing human α7 nAChRs; *bottom*, dose response curve for α7 nAChRs, $EC_{50} = 46.3$ μM, n = 5. **b** *Top*, typical whole-cell currents elicited by ACh and compound **3** 10 μM (*left* and *right*, respectively) on GH4C1 cells expressing human α4β2 nAChRs; *bottom*, dose response curve for α4β2 nAChRs, n = 4. **c** *Top*, typical whole-cell currents elicited by ACh and compound **3** 50 μM (*left* and *right*, respectively) on GH4C1 cells expressing human α3β4 nAChRs; *bottom*, dose response curve for α3β4 nAChRs, $EC_{50} = 5.2$ μM n = 6

functional profile at the α7, α4β2 and α3β4 nAChRs subtypes (Fig. 6), heterologously expressed in the rat anterior pituitary GH4C1 cell line. Functional expression of the different nAChRs was evaluated by measuring the whole-cell inward current elicited by ACh 1 mM, with mean current amplitudes of 32 ± 10 pA, 1,774 ± 437 pA and 6,945 ± 3,240 pA for α7, α4β2 and α3β4 nAChRs, respectively (n = 5,4,6, respectively; Fig. 6a–c). Derivative **3** was able to elicit significant inward currents when applied on GH4C1 cells expressing α7 and α3β4 nAChRs, with maximal responses representing 62 ± 8 % (at 200 μM; Fig. 6a) and 50 ± 5 % (at 50 μM; Fig. 6c) of ACh-induced current amplitudes, while its action on α4β2 nAChRs was markedly lower (8 ± 3 %, at 10 μM; Fig. 6b). Furthermore, for compound **3** the dose–response relationships indicated EC_{50} values of 46.3 μM and 5.2 μM for α7 and α3β4 nAChRs, respectively.

On the whole, these results point out that **3** behaves as a partial agonist at α3β4 and α7 nAChRs with different levels of potency, while its agonist action on α4β2 nAChRs is almost negligible. Moreover, it has to be stressed that simple insertion of the OH group in the skeleton of **2** brought about a dramatic loss of the efficacy of **3** at the α4β2 subtype, causing a drop of the maximal response from 112 [19] to 8 %.

Discussion

Several literature reports have investigated the relevance of water molecules as a source of additional hydrogen bond donor/acceptor sites contributing to the ligand-receptor mutual recognition. As far as nAChRs are concerned, the experimental data from Blum et al. [17] supported the role of a water molecule in mediating the interaction of the complementary receptor subunit with nicotinic agonists containing a hydrogen bond acceptor site. In our study, docking and MD analyses on potent nicotinic agonists such as epibatidine **1** and deschloroepibatidine **2** highlighted that a water molecule placed in the binding cavity of nAChR subtypes may generate distinct hydrogen bond interactions with the studied ligands. Moreover, we hypothesized a different location for this water molecule within the binding sites of the α3β4 and α4β2 nAChR models.

The binding affinity of **1** for the α4β2 receptor subtype was found to be lower than that of its analogue **2** lacking the chlorine atom, whereas an opposite behavior was shown by the two ligands at the α3β4 subtype. Moreover, Avalos et al. [19] reported that the effects on affinity of the "*para* substitution" of the pyridine ring in epibatidine-like ligands are comparable for the nAChR stoichiometries containing the same beta subunit. As illustrated in Table S2 (Supplementary Material), for a given ligand in the series the affinity measured at α4β2 nAChRs was similar to that found at α3β2 and α2β2 subtypes, and likewise the K_i values determined at α3β4, α2β4 and α4β4 nAChRs fell in the same range. Thus, β2-containing receptors give an overall response different from β4-containing receptors, suggesting that the substituent adjacent to the pyridine nitrogen projects towards a "complementary component" of the binding site, giving rise to an extra-interaction which modulates the ligand affinity for the different stoichiometries.

Moreover, the ligand affinity should be influenced by the pK_a value of the pyridine nitrogen atom, which affects the strength of the bond to be formed with a putative hydrogen donor. As far as the experimental binding data are compared with our computational results, the pK_a value of the pyridine nitrogen gives a major contribution to the interaction of **1** and **2** with the α4β2 protein, whereas exerts a minor role on the affinity of **2** in the α3β4 pocket. As a matter of fact, during the production phase of MD simulations on the α4β2 complexes, the water molecule was

found to be firmly bound to the pyridine nitrogen of **2**, while this interaction was lost in the same phase for the α3β4/**2** complex. Thus, the enhancement of α4β2 affinity on passing from **1** to **2** could be mainly attributed to the increase of pK_a value of the pyridine nitrogen, whereas this effect does not appear to influence the binding to the α3β4 subtype, where other factors should prevail. In fact, the simulations performed on the α3β4/**2** complex indicated that, without the chlorine anchoring effect, the pyridine ring of **2** acquires a higher degree of conformational mobility, since the average RMSF value was found to be 1.1 Å for **2** and 0.7 Å for **1** (Figure S1, Supplementary Material). This could be one of the causes responsible for the loss of the original pyridine-water hydrogen bond as well as the final different localization of the solvent molecule in the binding cleft of α3β4 and α4β2 receptors, thus promoting the reduction in affinity showed by **2** for the α3β4 subtype.

Based on the results of such computational investigation, we designed the deschloroepibatidine-related analogues **3** and **4**, whose hydroxyl groups could modify the pattern of interactions in the ligand binding area hosting the putative water molecule. Indeed, a theoretical investigation on the two new compounds allowed to hypothesize a different binding mode in their interaction with the α3β4 or α4β2 receptor subtypes and the water molecule. Following their synthesis and pharmacological evaluation, we observed a meaningful reduction of the affinity towards the α4β2 and α7 nAChR subtypes for **3** and **4** in comparison with the two reference ligands **1** and **2**. On the contrary, the K_i values of both **3** and **4** at the α3β4 subtype were closer to that known for their analogue **2**.

Hence, our theoretical and experimental results highlight that the novel nicotinic ligands **3** and **4** are able to perturb the hydrogen bond network formerly present in the solvated binding cleft, and it is plausible that the attempt to preserve their interaction with the water site results in an inversion of the α4β2 versus α3β4 nAChR selectivity profile. Indeed, deschloroepibatidine **2** is 1,290-fold more selective for the α4β2 over the α3β4 subtype, whereas its structural analogues **3** and **4** show an albeit low (1.6- and 4.7-fold) α3β4 versus α4β2 binding preference. Furthermore, in electrophysiological experiments **3** behaved as an α3β4 nAChR partial agonist, a profile found also at α7 nAChRs but not at α4β2 subtype, where this ligand elicited a negligible functional response.

In summary, after a theoretical investigation on reference compounds epibatidine **1** and its deschloro-analogue **2** within the α4β2, α3β4 and α7 nAChR models, we concluded that the presence of a water molecule in the receptor binding site is compatible with the experimental evidences. We tested our hypothesis designing and modeling the two novel deschloroepibatidine-related analogues **3** and **4**, in which the –OH and the –CH_2OH groups should theoretically perturb the interaction with the water molecule and, consequently, affect the affinity and the subtype selectivity profile of the resulting ligands. Following synthesis and pharmacological analysis, the two ligands revealed some degree of α3β4 versus α4β2 subtype selectivity. Therefore, replacing the pyridine nitrogen of deschloroepibatidine, a crucial structural element for the molecular recognition of nAChR agonists, with a suitable substitution pattern may represent a valuable approach to achieve α3β4 nAChR selective ligands, and these results encourage further efforts in this direction.

Experimental section

Docking and MD simulations

The α4β2, α3β4 and α7 nAChR models, previously developed by us [14, 22, 23], together with the **1** molecule retrieved from the crystal structure of *A*-AChBP/**1** (PDB accession code 2BYQ), were geometrically refined following the molecular modeling standard procedures: minimization, equilibration and molecular dynamics simulation. Ligands **1–4** were preliminarily minimized by Gaussian09 [31] at the DFT/B3LYP/6-31G(d) level. The partial charge of the ligand atoms was assigned by the RESP [32] method whereas, in accordance with the pK_a value of **1**, the net charge of all ligands was +1. Docking calculations were then performed with the GOLD 5.1 program [33] into the binding cleft depicted by α4-Trp147 and the homologue residues in the α3 and α7 subtypes. The cavity was detected with an active site radius of 12.0 Å from the carbonyl oxygen atom of the Trp residue. The PLP fitness function and the distribution of torsion angles were chosen to evaluate the quality of the docking results [34]. van der Waals and hydrogen bonding radii were set at 4.0 and 3.0 Å, respectively; genetic algorithm parameters were kept at the default value. Cluster analysis was performed by means of the GOLD internal algorithm, based on the RMSD of each pose compared with the one previously obtained. The solutions with the highest score belonging to the first cluster were visually inspected and then chosen for further analysis. The resulting complexes were submitted to molecular dynamics (MD) simulations with the *sander* and *pmemd* modules of the AMBER12 [35] package. *ff12* [35] and *GAFF* [36] force fields were applied for the protein and the ligands, respectively. The complexes were immersed in a box containing about 30,000 water molecules and the TIP3P model was employed to explicitly represent the solvent [37]. Na^+ counterions were added to maintain neutrality on the systems. At first, the energy of the water molecules was minimized, keeping the

atoms of the protein frozen. Then, a minimization of the whole system was performed by setting a convergence criterion on the gradient of 10^{-4} kcal mol^{-1} Å^{-1}. Prior to starting the MD simulations, the system was equilibrated for 40 ps at 300 K in isocore conditions (NVT). Subsequently, 10 ns of MD simulations in isothermal-isobaric ensemble were carried out at 300 K with a 2 fs time-step (NPT). In the production runs, the systems were performed in periodic boundary conditions. van der Waals and short-range electrostatic interactions were estimated within a 8 Å cutoff. SHAKE algorithm was applied to all bonds involving hydrogen atoms. When the geometrical stabilization of the complexes was reached, a new minimization of the whole system was performed.

Figures were acquired by the PyMOL software (The PyMOL Molecular Graphics System).

Chemistry

^{1}H NMR and ^{13}C NMR spectra were recorded with a Varian Mercury 300 (^{1}H, 300.063; ^{13}C, 75.451 MHz) spectrometer in $CDCl_3$ solutions (unless otherwise indicated) at 20 °C. Chemical shifts (δ) are expressed in ppm and coupling constants (J) in Hz. TLC analyses were performed on commercial silica gel 60 F_{254} aluminum sheets; spots were further evidenced by spraying with a dilute alkaline potassium permanganate solution or a phosphomolybdic acid solution and, for tertiary amines, with the Dragendorff reagent. Melting points were determined on a model B 540 Büchi apparatus and are uncorrected. ESI mass spectra were obtained on a Varian 320 LC–MS/MS instrument. Data are reported as mass-to-charge ratio (m/z) of the corresponding positively charged molecular ions. Microanalyses (C, H, N) agreed with the theoretical value within ±0.4 %.

(1R,2R*,4S*)-tert-Butyl-2-(3-methoxyphenyl)-7-azabicyclo[2.2.1]heptane-7-carboxylate* ***9***

To a stirred solution of alkene **6** [27] (157 mg, 0.804 mmol) in anhydrous DMF (3.5 mL) under an argon atmosphere, were added 1-bromo-3-methoxybenzene **7** (255 µL, 2.01 mmol), $Pd(OAc)_2$ (9 mg, 0.04 mmol), tetrabutylammonium chloride (56 mg, 0.201 mmol) and potassium formate (170 mg, 2.01 mmol). After heating at 80 °C for 5 h, the reaction mixture was cooled to room temperature, then poured into NH_4OH/H_2O (1:1, 10 mL) and extracted with dichloromethane (3 × 10 mL). The combined organic extracts were washed with brine (3 × 10 mL), then dried over anhydrous sodium sulfate, filtered and concentrated under reduced pressure. The residue was purified by silica gel column chromatography, eluting with cyclohexane/ethyl acetate (98:2) to yield 139 mg of the pure compound **9** (57 % yield).

9: Yellow oil. $R_f = 0.20$ (cyclohexane/ethyl acetate 9:1). ^{1}H NMR: 1.43 (s, 9H), 1.47–1.57 (m, 2H), 1.78–1.99 (m, 4H), 2.84 (dd, 1H, J = 5.5 and 8.8), 3.79 (s, 3H), 4.25 (bs, 1H), 4.35 (bs, 1H), 6.71–6.75 (m, 1H), 6.84–6.87 (m, 2H), 7.16–7.21 (m, 1H). ^{13}C NMR: 28.56, 29.02, 30.22, 40.77, 48.34, 55.30, 55.83, 62.25, 79.57, 111.83, 112.82, 119.71, 129.51, 147.68, 155.29, 159.89. MS (ESI) m/z $[M + H]^+$ Calcd for $C_{18}H_{25}NO_3$: 303.4. Found: 304.2. Anal. Calcd for $C_{18}H_{25}NO_3$ (303.40): C, 71.26; H, 8.31; N, 4.62. Found: C, 71.42; H, 8.66; N, 4.59.

(1R,2R*,4S*)-tert-Butyl-2-(3-hydroxyphenyl)-7-azabicyclo[2.2.1]heptane-7-carboxylate* ***10***

To a solution of **9** (118 mg, 0.389 mmol) in anhydrous dichloromethane (4.6 mL) at −78 °C under nitrogen was added a 1 M solution of boron tribromide in hexane (875 µL, 0.875 mmol) and stirring was continued for 1 h at −78 °C. After 2 h at 0 °C, the reaction was concentrated under vacuum and the residue was dissolved in dichloromethane (4 mL), alkalinized (pH = 9) by addition of triethylamine and then treated with di-*tert*-butyldicarbonate (170 mg, 0.778 mmol). The mixture was left under stirring for 2 h at room temperature, then diluted with a saturated $NaHCO_3$ aqueous solution (5 mL) and extracted with dichlorometane (3 × 3 mL). The combined organic extracts were washed with a 5 % H_3PO_4 aqueous solution (5 mL), then dried over anhydrous sodium sulfate, filtered and concentrated under reduced pressure. The residue was purified by silica gel column chromatography, eluting with cyclohexane/ethyl acetate (9:1) to yield 96 mg of the pure compound **10** (85 % overall yield).

10: Yellow oil. $R_f = 0.26$ (cyclohexane/ethyl acetate 7:3). ^{1}H NMR: 1.43 (s, 9H), 1.47–1.58 (m, 2H), 1.76–1.98 (m, 4H), 2.80–2.85 (m, 1H), 4.22 (bs, 1H), 4.35 (bs, 1H), 6.69–6.81 (m, 2H), 7.08–7.17 (m, 2H). ^{13}C NMR: 28.60, 29.17, 30.32, 39.70, 49.80, 55.40, 61.20, 80.17, 113.48, 119.19, 129.68, 147.36, 155.41, 156.68. MS (ESI) m/z $[M + H]^+$ Calcd for $C_{17}H_{23}NO_3$: 289.4. Found: 290.2. Anal. Calcd for $C_{17}H_{23}NO_3$ (289.37): C, 70.56; H, 8.01; N, 4.84. Found: C, 70.47; H, 8.37; N, 4.59.

(1R,2R*,4S*)-tert-Butyl-2-(3-(hydroxymethyl)phenyl)-7-azabicyclo[2.2.1]heptane-7-carboxylate* ***11***

According to the method described above for compound **9**, alkene **6** (156 mg, 0.80 mmol) was reacted with (3-bromophenyl)methanol **8** (240 µL, 2 mmol) to prepare 78 mg of the pure intermediate **11** (32 % yield).

11: Yellow oil. $R_f = 0.32$ (cyclohexane/ethyl acetate 1:1). ^{1}H NMR: 1.43 (s, 9H), 1.47–1.60 (m, 2H), 1.78–1.95 (m, 4H), 2.86 (dd, 1H, J = 5.5 and 8.5), 4.22 (bs, 1H), 4.35 (bs, 1H), 4.64 (s, 2H), 7.16–7.21 (m, 2H), 7.24–7.29 (m,

2H). ^{13}C NMR: 28.58, 29.93, 30.54, 40.75, 48.22, 54.60, 62.50 65.56, 79.74, 125.08, 125.99, 126.50, 128.85, 141.26, 146.30. MS (ESI) *m/z* $[M + H]^+$ Calcd for $C_{18}H_{25}NO_3$: 303.4. Found: 304.2. Anal. Calcd for $C_{18}H_{25}NO_3$ (303.40): C, 71.26; H, 8.31; N, 4.62. Found: C, 71.12, H, 8.68, N, 4.37.

3-{(1R,2R*,4S*)-7-Azabicyclo[2.2.1]heptan-2-yl}phenol hydrochloride* ***3 × HCl***

To a solution of the *N*-Boc protected derivative **10** (82 mg, 0.284 mmol) in diethyl ether (0.4 mL) was added a 4 N solution of HCl in dioxane (0.660 mL, 2.64 mmol) at 0 °C. The mixture was stirred at room temperature for 4 h and then the volatiles were removed under vacuum. The thick oily residue was taken up with anhydrous diethyl ether and repeatedly dried under vacuum to quantitatively afford the desired hydrochloride.

3 × HCl: Colorless hygroscopic prisms. ^{1}H NMR (CD_3OD): 1.83–2.12 (m, 5H), 2.37 (dd, 1H, $J = 9.4$ and 13.4), 3.29–3.34 (m, 1H), 4.28 (bs, 1H), 4.44 (bs, 1H), 6.66–6.79 (m, 3H), 7.18 (t, 1H, $J = 8.0$). ^{13}C NMR (CD_3OD): 25.73, 27.52, 36.46, 44.74, 59.21, 63.28, 113.59, 113.77, 117.23, 129.88, 142.98, 157.92. MS (ESI) *m/z* $[M + H]^+$ Calcd for $C_{12}H_{15}NO$: 189.3. Found: 190.1. Anal. Calcd for $C_{12}H_{16}ClNO$ (225.71): C, 63.85; H, 7.14; N, 6.21. Found: C, 63.56; H, 7.41; N, 6.01.

{3-((1R,2R*,4S*)-7-Azabicyclo[2.2.1]heptan-2-yl)phenyl}methanol hydrochloride* ***4 × HCl***

According to the procedure described above for derivative **3**, the *N*-Boc derivative **11** (60 mg, 0.198 mmol) was treated with hydrochloric acid to provide quantitatively the corresponding hydrochloride.

4 × HCl: Colorless hygroscopic prisms. ^{1}H NMR (CD_3OD): 1.86–2.18 (m, 5H), 2.41 (dd, 1H, $J = 9.4$ and 13.4), 3.40 (dd, 1H, $J = 6.1$ and 9.4), 4.29 (m, 1H), 4.47 (m, 1H), 4.62 (s, 2H), 7.20–7.38 (m, 4H). ^{13}C NMR (CD_3OD): 25.76, 27.53, 36.44, 44.82, 59.25, 63.35, 63.83, 125.05, 125.38, 125.56, 128.88, 141.50, 142.28. MS (ESI) *m/z* $[M + H]^+$ Calcd for $C_{13}H_{17}NO$: 203.28. Found: 204.0. Anal. Calcd for $C_{13}H_{18}ClNO$ (239.74): C, 65.13; H, 7.57; N, 5.84. Found: C, 64.87; H, 7.91; N, 5.63.

Receptor binding assays

Membranes binding of [^{3}H]epibatidine and [^{125}I]α-bungarotoxin

Frozen cortex and hippocampus specimens taken from adult male Sprague–Dawley rats (Charles River, Calco Italy) were homogenised using a Potter homogenizer in an excess of buffer A (50 mM Tris–HCl, pH 7, 120 mM NaCl, 5 mM KCl, 1 mM $MgCl_2$ and 2.5 mM $CaCl_2$ and 2 mM phenylmethylsulfonyl fluoride), centrifuged (60 min at 30,000×*g*), and rinsed twice. The homogenates were resuspended in the same buffer containing 20 μg/mL of the protease inhibitors leupeptin, bestatin, pepstatin A, and aprotinin.

[^{3}H]-epibatidine binding to cortical α4β2 and [^{125}I]-α-Bungarotoxin binding to hippocampal α7 membrane-subtypes were performed as previously described [38].

Binding to heterologously expressed α3β4 receptors

HEK 293 cells were grown in Dulbecco's modified Eagle medium supplemented with 10 % fetal bovine serum, 1 % L-Glutamine, 100 units/mL penicillin G, and 100 μg/ streptomycin in a humidified atmosphere containing 10 % CO_2. The cDNAs encoding α3 and β4 were transfected into the HEK 293 cells at 30 % confluency. The cell transfections were performed in 100 mm Petri dishes using 30 μL of JetPEI^{TM} (Polypus, France) (1 mg/mL, pH 7.2) and 10 μg of cDNAs. After 48 h transfection, the cells were collected, washed with PBS by centrifugation, and used for binding analysis.

nACh Receptor affinity of compounds ***3*** *and* ***4***

The inhibition of radioligand binding by epibatidine and the test compounds was measured by pre-incubating cortex homogenates with increasing doses (10 pM–10 mM) of the reference nicotinic agonists, epibatidine or nicotine, and the drug to be tested for 30 min at r.t., followed by overnight incubation with a final concentration of 0.100 nM [^{3}H]-epibatidine or 1 nM [^{125}I]-α-bungarotoxin at the same temperatures as those used for the saturation experiments. These ligand concentrations were used for the competition binding experiments because they are within the range of the K_D values of the ligands for the different classes of nAChRs. For each compound, the experimental data obtained from the three saturation and three competition-binding experiments were analyzed by means of a non-linear least square procedure, using the LIGAND program as described by Munson and Rodbard [30]. The binding parameters were calculated by simultaneously fitting three independent saturation experiments and the K_i values were determined by fitting the data of three independent competition experiments. The errors in the K_D and K_i values of the simultaneous fits were calculated using the LIGAND software, and were expressed as percentage coefficients of variation (% CV). When final compound concentrations up to 100 μM did not inhibit radioligand binding, the K_i value was defined as being >100 μM based on the Cheng and Prusoff's equation [39].

Binding to HEK 293 transfected α3β4 receptors was performed by overnight incubation at 4 °C with [^{3}H]epibatidine at a concentration ranging from 0.005 to 1 nM. All of the incubations were performed in a buffer containing 50 mM Tris–HCl, pH 7, 150 mM NaCl, 5 mM KCl, 1 mM $MgCl_2$, 2.5 mM $CaCl_2$, 2 mg/mL BSA. Specific ligand binding was defined as total binding minus the binding in the presence of 100 nM cold epibatidine. The inhibition of [^{3}H]epibatidine binding by compounds was measured by incubating increasing concentration of the compounds for 5 min followed by overnight incubation with 0.25 nM. After incubation, the membranes of HEK cells transfected with α3β4 receptors were washed four times with ice-cold PBS, and the bound [^{3}H]epibatidine was then determined by means of liquid scintillation counting in a β counter.

Electrophysiological recordings

The human α7, α4β2 and α3β4 nAChRs were expressed by transient transfection in the rat anterior pituitary GH4C1 cell line [40]. Transient transfection was achieved by adding to each dish 1 μg of the subunit cDNAs, along with 4 μL/μg of lipofectamine. All culture media were purchased from Invitrogen (San Giuliano Milanese, Italy). Whole-cell current recordings were performed 2–3 days after plating. Recordings and data analysis were performed by using borosilicate glass patch pipette (3- to 6-MΩ tip resistance) connected to an Axopatch 200A amplifier (Axon Instruments, Foster City, CA). Data were stored on a PC computer by using PCLAMP10 software (Molecular Devices). During the recording period, the cells were bathed in the following solution (mM): 140 NaCl, 2 $CaCl_2$, 2.8 KCl, 2 $MgCl_2$, 10 Hepes/NaOH and 10 glucose; pH 7.3. The patch pipettes were filled with a solution containing (mM): 140 CsCl, 2 MgATP, 10 Hepes/CsOH and 5 BAPTA; pH 7.3. Whole-cell capacitance and patch series resistance (3–5 MΩ) were estimated from slow transient compensations. A series resistance compensation of 85–90 % was obtained in all cases. The cells were voltage-clamped at a holding potential of −70 mV and continuously perfused with a gravity-driven system using independent external tubes for the control and agonist-containing solutions. These tubes were positioned 50–100 μm from the patched cell and connected to a fast exchanger system (RSC-160, BioLogic, France). Dose–response relationships were construct by sequentially applying different concentrations of agonists, and normalizing the obtained current amplitudes to the value obtained by applying 1 mM ACh on the same cell. For quantitative estimations of agonist actions, dose–response relationship were fitted to the Eq. (1):

$$I = I_{\max}\{[C]^{nH}/(EC_{50}^{nH} + [C]^{nH})\} \quad (1)$$

where I is the current amplitude induced by the agonist at concentration [*C*], I_{max} is the maximum response of the cell, nH is the Hill coefficient and EC_{50} is the concentration for which a half maximum response is induced.

Acknowledgments This research was supported by the Italian MIUR (PRIN 2009-R7WCZS), the CNR Research Project on Aging, the Regione Lombardia Project NUTEC ID 30263049 and the *Fondazione Giancarla Vollaro*, Milano. We acknowledge the CINECA and the Regione Lombardia award under the LISA initiative, for the availability of high performance computing resources and support. Carlo Matera wishes to thank "Dote Ricerca": FSE, Regione Lombardia, which co-financed his postdoctoral position.

References

1. Dajas-Bailador F, Wonnacott S (2004) Nicotinic acetylcholine receptors and the regulation of neuronal signaling. Trends Pharmacol Sci 25:317–324
2. Fenster CP, Rains MF, Noerager B, Quick MW, Lester RAJ (1997) Influence of subunit composition on desensitization of nicotinic receptors at low concentrations of nicotine. J Neurosci 17:5747–5759
3. Nai Q, McIntosh JM, Margotta JF (2003) Relating neuronal nicotinic acetylcholine receptor subtypes defined by subunit composition and channel function. Mol Pharmacol 63:311–324
4. Gotti C, Clementi F (2004) Neuronal nicotinic receptors: from structure to pathology. Prog Neurobiol 74:363–396
5. Jensen AA, Frølund B, Liljefors T, Krogsgaard-Larsen P (2005) Neuronal nicotinic acetylcholine receptors: structural revelations, target identifications, and therapeutic inspirations. J Med Chem 48:4705–4745
6. Lindström J (1997) Nicotinic acetylcholine receptors in health and desease. Mol Neurobiol 15:193–222
7. Paterson D, Nordberg A (2000) Neuronal nicotinic receptors in the human brain. Prog Neurobiol 61:75–111
8. Lloyd GK, Williams M (2000) Neuronal nicotinic acetylcholine receptors as novel drug targets. J Pharmacol Exp Ther 292:461–467
9. Hansen SB, Sulzenbacher G, Huxford T, Marchot P, Taylor P, Bourne Y (2005) Structures of Aplysia AChBP complexes with nicotinic agonists and antagonists reveal distinctive binding interfaces and conformations. EMBO J 24:3635–3646
10. Celie PH, van Rossum-Fikkert SE, van Dijk WJ, Brejc K, Smit AB, Sixma TK (2004) Nicotine and carbamylcholine binding to nicotinic acetylcholine receptors as studied in AChBP crystal structures. Neuron 41:907–914
11. Billen B, Spurny R, Brams M, van Elk R, Valera-Kummer S, Yakel JL, Voets T, Bertrand D, Smit AB, Ulens C (2012) Molecular actions of smoking cessation drugs at α4β2 nicotinic receptors defined in crystal structures of a homologous binding protein. Proc Natl Acad Sci USA 109:9173–9178
12. Le Novère N, Grutter T, Changeux JP (2002) Models of the extracellular domain of the nicotinic receptors and of agonist- and Ca2 + -binding sites. Proc Natl Acad Sci USA 99:3210–3215
13. Schapira M, Abagyan R, Totrov M (2002) Structural model of nicotinic acetylcholine receptor isotypes bound to acetylcholine and nicotine. BMC Struct Biol 2:1
14. Mazzo F, Pistillo F, Grazioso G, Clementi F, Borgese N, Gotti C (2013) Nicotine-modulated subunit stoichiometry affects stability and trafficking of α3β4 nicotinic receptor. J Neurosci 33:12316–12328

15. Wang HL, Gao F, Bren N, Sine SM (2003) Curariform antagonists bind in different orientations to the nicotinic receptor ligand binding domain. J Biol Chem 278:32284–32291
16. Amiri S, Sansom MSP, Biggin PC (2007) Molecular dynamics studies of AChBP with nicotine and carbamylcholine: the role of water in the binding pocket. Protein Eng Des Sel 20:353–359
17. Blum AP, Lester HA, Dougherty DA (2010) Nicotinic pharmacophore: the pyridine N of nicotine and carbonyl of acetylcholine hydrogen bond across a subunit interface to a backbone NH. Proc Natl Acad Sci USA 107:13206–13211
18. Blum AP, Van Arnam EB, German LA, Lester HA, Dougherty DA (2013) Binding interactions with the complementary subunit of nicotinic receptors. J Biol Chem 288:6991–6997
19. Avalos M, Parker MJ, Maddox FN, Carrol FI, Luetje CW (2002) Effects of pyridine ring substitutions on affinity, efficacy, and subtype selectivity of neuronal nicotinic receptor agonist epibatidine. J Pharm Exp Ther 302:1246–1252
20. Huang X, Zheng F, Crooks PA, Dwoskin LP, Zhan C (2005) Modeling multiple species of nicotine deschloroepibatidine interacting with α4β2 nicotinic acetylcholine receptor: from microscopic to phenomenological binding affinity. J Am Chem Soc 127:14401–14414
21. Abin-Carriquiry JA, Zunini MP, Cassels BK, Wonnacott S, Dajas F (2010) In silico characterization of cytisinoids docked into an acetylcholine binding protein. Bioorg Med Chem Lett 20:3683–3687
22. Grazioso G, Pomè DY, Matera C, Frigerio F, Pucci L, Gotti C, Dallanoce C, De Amici M (2009) Design of novel alpha7-subtype-preferring nicotinic acetylcholine receptor agonists: application of docking and MM-PBSA computational approaches, synthetic and pharmacological studies. Bioorg Med Chem Lett 19:6353–6357
23. Grazioso G, Cavalli A, De Amici M, Recanatini M, De Micheli C (2008) Alpha7 nicotinic acetylcholine receptor agonists: prediction of their binding affinity through a molecular mechanics Poisson-Boltzmann surface area approach. J Comp Chem 29:2593–2602
24. Carroll FI (2004) Epibatidine structure–activity relationships. Bioorg Med Chem Lett 14:1889–1896
25. Linnel RH (1960) Dissociation constants of 2-substituted pyridines. J Org Chem 25:290
26. Nalam MN, Peeters A, Jonckers TH, Dierynck I, Schiffer CA (2007) Crystal structure of lysine sulfonamide inhibitor reveals the displacement of the conserved flap water molecule in human immunodeficiency virus type 1 protease. J Virol 81:9512–9518
27. Carroll FI, Liang F, Navarro HA, Brieaddy LE, Abraham P, Damaj MI, Martin BR (2001) Synthesis, nicotinic acetylcholine receptor binding, and antinociceptive properties of 2-*exo*-2-(2′-substituted 5′-pyridinyl)-7-azabicyclo[2.2.1]heptanes. Epibatidine analogues. J Med Chem 44:2229–2237
28. Carroll FI, Ma W, Yokota Y, Lee JR, Brieaddy LE, Navarro HA, Damaj MI, Martin BR (2005) Synthesis, nicotinic acetylcholine receptor binding, and antinociceptive properties of 3′-substituted deschloroepibatidine analogues. novel nicotinic antagonists. J Med Chem 48:1221–1228
29. Kasyan A, Wagner C, Maier ME (1998) Regiochemistry of the reductive heck coupling of 2-azabicyclo[2.2.1]hept-5-ene. Synthesis of epibatidine analogues. Tetrahedron 54:8047–8054
30. Munson PJ, Rodbard D (1980) Ligand: a versatile computerized approach for characterization of ligand-binding systems. Anal Biochem 107:220–239
31. Frisch MJ, Trucks GW, Schlegel HB, Scuseria GE, Robb MA, Cheeseman JR, Scalmani G, Barone V, Mennucci B, Petersson GA, Nakatsuji H, Caricato M, Li X, Hratchian HP, Izmaylov AF, Bloino J, Zheng G, Sonnenberg JL, Hada M, Ehara M, Toyota K, Fukuda R, Hasegawa J, Ishida M, Nakajima T, Honda Y, Kitao O, Nakai H, Vreven T, Montgomery JJA, Peralta JE, Ogliaro F, Bearpark M, Heyd JJ, Brothers E, Kudin KN, Staroverov VN, Kobayashi R, Normand J, Raghavachari K, Rendell A, Burant JC, Iyengar SS, Tomasi J, Cossi M, Rega N, Millam NJ, Klene M, Knox JE, Cross JB, Bakken V, Adamo C, Jaramillo J, Gomperts R, Stratmann RE, Yazyev O, Austin AJ, Cammi R, Pomelli C, Ochterski JW, Martin RL, Morokuma K, Zakrzewski VG, Voth GA, Salvador P, Dannenberg JJ, Dapprich S, Daniels AD, Farkas Ö, Foresman JB, Ortiz JV, Cioslowski J, Fox DJ (2009) Gaussian 09, revision A.02. Gaussian, Inc., Wallingford, CT
32. Liu YP (2001) Applications of effective core potentials and density functional theory to the spin states of iron porphyrin. J Chem Inf Comput Sci 41:22–29
33. Gold v. 5.1. Cambridge Crystallographic Data Centre, Cambridge, UK
34. Korb O, Stutzle T, Exner TE (2009) Empirical scoring functions for advanced protein-ligand docking with PLANTS. J Chem Inf Model 49:84–96
35. Case DA, Darden TA, Cheatham TEIII, Simmerling CL, Wang J, Duke RE, Luo R, Walker C, Zhang W, Merz KM, Roberts B, Hayik S, Roitberg A, Seabra G, Swails J, Goetz AW, Kolossváry I, Wong KF, Paesani F, Vanicek J, Wolf RM, Liu J, Wu X, Brozell SR, Steinbrecher T, Gohlke H, Cai Q, Ye X, Wang J, Hsieh MJ, Cui G, Roe DR, Mathews DH, Seetin MG, Salomon-Ferrer R, Sagui C, Babin V, Luchko T, Gusarov S, Kovalenko A, Kollman PA (2012) AMBER 12. University of California, San Francisco
36. Wang J, Wolf RM, Caldwell JW, Kollman PA, Case DA (2004) Development and testing of a general amber force field. J Comput Chem 25:1157–1174
37. Jorgensen WL, Chandrasekhar J, Madura JD, Impey RW, Klein LM (1983) Comparison of simple potential functions for simulating liquid water. J Chem Phys 79:926–936
38. Carbonelle E, Sparatore F, Canu-Boido C, Salvagno C, Baldani-Guerra B, Terstappen G, Zwart R, Vijverberg H, Clementi F, Gotti C (2003) Eur J Pharmacol 471:85–96
39. Cheng Y, Prusoff WH (1973) Relationship between the inhibition constant (K1) and the concentration of inhibitor which causes 50 per cent inhibition (I50) of an enzymatic reaction. Biochem Pharmacol 22:3099–3108
40. Fucile S, Renzi M, Lax P, Eusebi F (2003) Cell Calcium 34:205–209
41. Parker MJ, Beck A, Luetje CW (1998) Neuronal nicotinic receptor beta2 and beta4 subunits confer large differences in agonist binding affinity. Mol Pharmacol 54:1132–1139
42. Sullivan JP, Donnelly-Roberts D, Briggs CA, Anderson DJ, Gopalakrishnan M, Piattoni-Kaplan M, Campbell JE, McKenna DG, Molinari E, Hettinger AM, Garvey DS, Wasicak JT, Holladay MW, Williams M, Arneric SP (1996) A-85380 [3-(2(S)-azetidinylmethoxy) pyridine]: in vitro pharmacological properties of a novel, high affinity alpha 4 beta 2 nicotinic acetylcholine receptor ligand. Neuropharmacology 35:725–734